

# Nanoscale

Accepted Manuscript



This is an *Accepted Manuscript*, which has been through the Royal Society of Chemistry peer review process and has been accepted for publication.

*Accepted Manuscripts* are published online shortly after acceptance, before technical editing, formatting and proof reading. Using this free service, authors can make their results available to the community, in citable form, before we publish the edited article. We will replace this *Accepted Manuscript* with the edited and formatted *Advance Article* as soon as it is available.

You can find more information about *Accepted Manuscripts* in the [Information for Authors](#).

Please note that technical editing may introduce minor changes to the text and/or graphics, which may alter content. The journal's standard [Terms & Conditions](#) and the [Ethical guidelines](#) still apply. In no event shall the Royal Society of Chemistry be held responsible for any errors or omissions in this *Accepted Manuscript* or any consequences arising from the use of any information it contains.

## ARTICLE

## Enhanced radiation therapy with internalized polyelectrolyte modified nanoparticles

Cite this: DOI: 10.1039/x0xx00000x

Peipei Zhang, Yong Qiao, Chaoming Wang, Liyuan Ma\*, Ming Su\*,

Received 00th January 2012,  
Accepted 00th January 2012

DOI: 10.1039/x0xx00000x

www.rsc.org/

**Abstract:** A challenge of X-ray radiation therapy is that high dose X-ray at therapeutic condition damages normal cells. This paper describes a nanoparticle-based method to enhance X-ray radiation therapy by delivering radio-sensitizing gold nanoparticles into cancer cells. The nanoparticles have been modified with cationic polyelectrolytes to allow internalization. Upon X-ray irradiation of nanoparticles, more photoelectrons and Auger electrons are generated to cause water ionization, leading to formation of free radicals that damage DNA of cancer cells. The X-ray dose required for DNA damage and cell killing is reduced by putting gold nanoparticles inside cancer cells.

### Introduction

X-ray photons in radiation therapy can generate photoelectrons and Auger electrons, which can cause ionization of water and formation of reactive free radicals (mostly hydroxyl radicals). The free radicals diffuse through chain reactions in cells, and damage DNA in mitochondria and nuclei by extracting hydrogen atoms from ribose sugars, leading to cleavage of polynucleotide backbone.<sup>1-9</sup> A challenge of X-ray radiation therapy is that high dose X-ray can damage normal cells and cause side effects due to its low tumor selectivity.<sup>10</sup> Nanoparticles of gold,<sup>11-13</sup> platinum<sup>14</sup> or bismuth<sup>15, 16</sup> have been proposed to enhance radiation therapy, but the measured effect of nanoparticles is negligible.<sup>17-19</sup> This is likely due to the fact that these nanoparticles are attached on cell membrane, and X-ray generated free radicals have to diffuse into vicinity of DNA to cause damage.<sup>19</sup> If radiosensitizers could be placed in cancer cells or nuclei, the amount of free radicals available for DNA damage will be enhanced, and the total X-ray dose could be reduced to receive the same treatment effect.<sup>19</sup>

The cell membrane penetrating ability of nanoparticles depends on sizes, shapes and surface properties such as charge and hydrophobicity.<sup>20-23</sup> Nanoparticles that are modified with positively charged molecules can be attracted on negatively charged cell surface, and taken by cells via endocytosis.<sup>24</sup> Layer-by-layer assembly allows controlled surface modification of nanoparticles by depositing polyelectrolytes of opposite charges.<sup>25</sup> The surface charge of nanoparticle is controlled by the amount of polyelectrolyte adsorbed on outmost surface, providing a facile and effective way of optimizing the cellular uptake efficiency. This paper describes a new way to enhance X-ray radiation killing of aggressive cancer cells by internalizing gold nanoparticles into cancer cells (Fig. 1A), where alternating cationic and anionic polyelectrolyte are used to modify gold nanoparticles (Fig. 1B). It is found gold nanoparticles with positive charges show enhanced intracellular delivery into cells and these nanoparticles do not affect

cell viability. Upon X-ray irradiation, cells with internalized positively-charged gold nanoparticles show higher level of DNA damage and susceptibility to be killed, compared to those negatively charged nanoparticles that are not internalized.

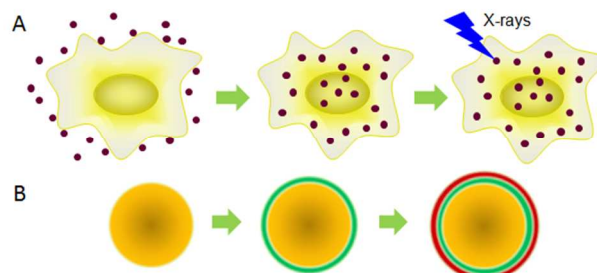


Figure 1. Cell-penetrating nanoparticles for enhanced X-ray radiation therapy (A); Nanoparticles modified with polyelectrolyte multilayers (B).

### Experimental Section

Polyethylenimine (PEI) (10,000 Da), polysodium 4-styrene sulfonate (PSS) (70,000 Da), and polydiallyl-dimethyl ammonium chloride (PDAC) (100,000-200,000 Da) were from Aldrich. Polydimethylsiloxane (PDMS Sylgard 184) was from Dow-Corning. PDMS stamps were prepared by casting PDMS pre-polymer and curing agent on solid masters made by photo-lithography. Rhodamine isothiocyanate (RITC), fluorescein isothiocyanate (FITC), propidium iodide (PI) and gold nanoparticles were from Sigma. SYBR green fluorescence dye was from Invitrogen.

PEI was labeled with FITC or RITC by reacting with FITC or RITC in water at a 3000:1 molar ratio (PEI repeat units and dye molecules) for 24 h at room temperature. Gold nanoparticles and polyelectrolyte were used at concentrations of  $1.0 \times 10^{10}$  nanoparticles  $\text{mL}^{-1}$ , and  $5.0 \text{ mg mL}^{-1}$ , respectively. To coat nanoparticles with polyelectrolytes, the nanoparticle suspension was added drop-wise into PEI-RITC solution. The modified nanoparticles were collected by centrifugation, and then added in PSS solution. The steps were repeated until a desired number layer was formed around nanoparticles. Human glioblastoma cells (A712) were cultured in RPMI 1640 medium supplemented with 10% (v/v) cosmic calf serum, 100 units  $\text{mL}^{-1}$  of penicillin, and 100  $\text{mg mL}^{-1}$  streptomycin at  $37^\circ\text{C}$  and 5%  $\text{CO}_2$ . Polyelectrolyte modified nanoparticles were added in culture medium at nanoparticles-to-cell ratio of 100. After incubation for 24 h, cells were washed with phosphate buffered saline (PBS)(1 $\times$ ) to remove excess nanoparticles.

Live dead assay was performed to cells with gold nanoparticles with LIVE/DEAD® kit (Life Technologies) according to the instructions provided by the company. An Accuri C6 cytometer (BD Bioscience Inc.) equipped with an air-cooled laser (20 mW) at 488 and 640 nm with the standard filter setup was used for flow cytometry assay. For cell cycle analysis, cells were fixed in 3 mL 100% ethanol, and DNAs were stained with 0.4 mL PI (0.5% PI in PBS with 0.1% Triton X-100) and assessed with flow cytometry. Histogram was analyzed by defining borders of different phases of cell cycle (G0/G1, G2, S, and M). Mean fluorescence intensity (MFI) of cells was measured by the software equipped with the machine. The production of free radicals was assessed with Image-iT™ LIVE Green Reactive Oxygen Species (ROS) detection kit (Life Technology Inc.) using a fluorescent marker, 5-(-6)-carboxy-2,7-dichlorodihydro-fluorescein diacetate (carboxy H2 DCFDA), which permeates live cells, and can be deacetylated by non-specific intracellular esterases. The deacetylated fluorogenic marker can generate green color under fluorescence microscope.

DNA damage was measured with alkaline halo assay.<sup>26</sup> Briefly, cells exposed to X-ray or nanoparticles were patterned to form single cell array on glass substrate, and embedded in 0.1% (mass ratio) agarose gel. After gel solidification, the slide was incubated with 0.3 M NaOH for 15 min at room temperature, and stained with 10  $\mu\text{g/mL}$  SYBR for 10 min. The slide was incubated in deionized water for 3 min to remove excess SYBR. Phase contrast and epifluorescence images were collected with 40X and 10X objectives on an inverted microscope (Olympus IX83). DNA double strand break was assessed with expression of DNA repair protein,  $\gamma\text{-H2XA}$ . Briefly, A172 cells with different treatment were fixed with 4% paraformaldehyde in PBS for 20 min, and treated with 0.1% Triton X-100 in PBS for 5 min. After incubating in blocking buffer (3% bovine serum albumin in PBS) for 1 h, primary antibodies against  $\gamma\text{-H2XA}$  were added to cells, and incubated at room temperature for 2 h. After rinsing with PBS, cells were incubated with FITC-conjugated secondary antibody (anti-rabbit IgG-FITC antibody produced in goat) for 1 h and washed with PBS, and stained with 0.2  $\mu\text{g/mL}$  DAPI for 15 min and washed with PBS. Fluorescence intensity of the secondary antibody labeled cells was measured with 96 well plate reader under an excitation light of 488 nm (PerkinElmer 1420 multilabel counter 1420). Electrophoresis was done at alkaline conditions, where cells were treated with 0.3 M alkaline solution for 10 min (pH 13).

## Results and discussions

Fig. 2A is a transmission electron microscopy (TEM) image of gold nanoparticles, which have an average diameter of  $13.5 \pm 1.3 \text{ nm}$ . The

nanoparticles are modified with three layers of polyelectrolytes, i.e., PEI, PSS, and PEI. To confirm presence of multilayer, two fluorescent dyes, i.e., green colored FITC and red colored RITC are incorporated in the inner-most PEI layer and outmost PEI layer, respectively, as shown in fluorescence microscopy images (Fig. 2B and 2C). Fig. 2D is a merged image collected with TRITC and FITC filters of fluorescence microscope. The yellow color confirms existence of PEI-RITC and PEI-FITC on nanoparticles. Zeta potential of nanoparticles has been measured after addition of each layer (Fig. 2E). A reversal of surface charge following the deposition of each layer is clear. The size distribution of nanoparticles has been tested with dynamic light scattering. The sizes of nanoparticles increase with the number of layer (Fig. 2F). When the number of layers is over 4, the formation of polyelectrolyte bridges (flocculation) between adjacent nanoparticles brings nanoparticles closer, causing large size variation (135 nm) (Fig. 2G). Ultraviolet-visible spectrometer is used to characterize nanoparticles modified with 1 to 5 layers of polyelectrolytes. A red shift of absorption peak to long wavelength reflects the deposition of polyelectrolyte layer, which changes dielectric constants around nanoparticles.

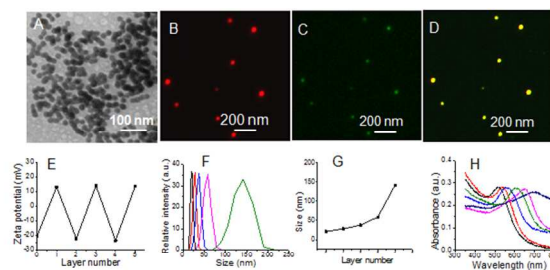


Figure 2. TEM image of gold nanoparticles (A); Fluorescence images of nanoparticles under TRITC (B) and FITC filter (C); Merged picture of images collected with TRITC and FITC filter (D); Zeta potential (E), and dynamic light scattering (F) results of nanoparticles after addition of each polyelectrolyte layer; Maximum size of polyelectrolyte modified nanoparticles (G); UV-Vis spectra of nanoparticles after adding each layer of polyelectrolyte (H).

PEI coated positively charged nanoparticles are added in the culture medium of A172 cells. After 24 h, cell viability test shows cells are green, indicating cells are alive (Fig. 3A), where red color is from PEI-RITC modified nanoparticles. The location of nanoparticles relative to cells is tested with phase contrast imaging (Fig. 3B) and fluorescent imaging (Fig. 3C). The merged image indicates nanoparticles are adjacent to cells (Fig. 3D). To determine whether nanoparticles are internalized in cell or not, cells have been imaged at focal length of  $7.5 \mu\text{m}$  using confocal microscope. Fig. 3E shows some nanoparticles are in the same focus plane. Fluorescence image indicates 92.8% of cells have internalized nanoparticles. Fluorometry result shows that  $\sim 81$  nanoparticles are internalized in each cell. In comparison, negatively charged nanoparticles with PSS at outmost layer are not taken up by cells at all (Fig. 3F), where no nanoparticles can be found inside cells, and the arrows show nanoparticles left after washing. In order to determine whether internalized nanoparticles affect cell cycle, cells with and without internalized nanoparticles are stained with propidium iodide (PI), and analyzed with flow cytometry. Fig. 3G and 3H show similar distribution in cell number-fluorescent intensity plots of both samples: 72.3% cells with internalized nanoparticles and 71.9% cells without internalized nanoparticles are in G0/G1, suggesting that internalization does not change cell cycles.

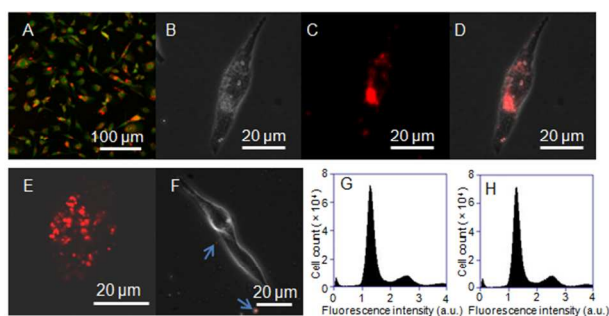


Figure 3. Live/Dead assay of cells with nanoparticles (A); Phase contrast (B) and fluorescence (C) images of cells with nanoparticles; Merged phase contrast and fluorescence images (D); Confocal fluorescence image of cells with nanoparticles in z stack at 7.5  $\mu\text{m}$  under cell surface (E); Interaction of negatively charged nanoparticles with A172 cells (F); Flow cytometry analysis of cell cycle of cells without nanoparticles (G), and with nanoparticles (H).

The production of free radicals in cells after X-ray irradiation (40 kV, 100  $\mu\text{A}$ , and 80 mGy/min) is indicated in a fluorescence image using carboxy H2 DCFDA probe. Fig. 4A shows strong green fluorescence emission and a high level of free radicals from cells with internalized charged nanoparticles. An enlarged image shows the co-existence of fluorescently labelled nanoparticles (red color), DAPI stained nucleus (blue), and free radical generated green fluorescence from each cell (Fig. 4B). Flow cytometry is used to quantify free radicals in four sets of samples: cells with negatively charged (1) or internalized (2) nanoparticles; cells with negatively charged nanoparticles and X-ray (3); cells with internalized nanoparticles and X-ray (4). Fig. 4C and 4D show that there is almost no detectable fluorescence signal from sample (1) and (2). MFI in sample (4) ( $5.0 \times 10^6$ ) is 3 times stronger than that of sample (3) ( $1.6 \times 10^6$ ) (Fig. 4E and 4F). DNA damages in the four samples are assessed by electrophoresis, where cells are treated with 0.3 M NaOH for 10 min, and DNAs are stained with ethidium bromide (EB). DNA damages are quantified by distances that DNA fragments move in gel electrophoresis. Fig. 4G shows that DNAs in sample (1) and (2) have moved a similar distance, indicating that DNA damage levels in both samples are similar. DNAs from X-ray irradiated cells with internalized nanoparticles move a longer distance than those from cells without internalized nanoparticles.

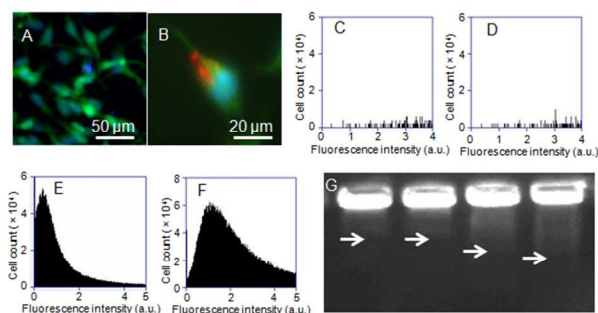


Figure 4. Fluorescence image (A) and an enlarged image (B) of ROS stained cells that have internalized nanoparticles; Flow cytometry results: cells with (C) and without (D) internalized nanoparticles without X-ray; Cells without (E) and with (F) internalized nanoparticles with X-ray; Gel electrophoresis results of four samples (bands from left to right are from sample 1 to sample 4) (G).

DNA damage in each sample has been quantified using PI stained DNAs as a marker with flow cytometry. Cells in different phases have different amount of DNA: normal cells in G0/G1 phase have 1 unit of DNA content; those in S phase have increased DNA content due to duplication; upon entering G2 phase and later M phase, DNA content is doubled (2 units). Cells are irradiated with X-ray for 15 minutes, and put back to incubator for 48 h. The fluorescence intensity corresponding to no DNA damage is set at 1 unit; those lower than 1 unit is caused by either apoptosis or DNA damaged into smaller fragments. Fig. 5A and 5B are flow cytometry results of X-ray irradiated cells with negatively charged nanoparticles and internalized nanoparticles, respectively. 38.8% cells with negatively charged nanoparticles and 72.4% cells with internalized nanoparticles show fluorescent intensity below 1 unit, suggesting internalized nanoparticles can enhance X-ray induced DNA damage. Fig. 5C shows the MFI of each sample: cells with negatively charged nanoparticles alone ( $1.38 \times 10^6$ ), cells with negatively charged nanoparticles and X-ray ( $1.25 \times 10^6$ ), and cells with internalized nanoparticles and X-ray ( $0.82 \times 10^6$ ). Cell death (apoptosis) after different treatment has also been determined using flow cytometry. A certain amount of cells ( $10^6$ ) with internalized positively charged nanoparticles is exposed to X-ray irradiation for different time, and cultured in medium for 48 h. Dead cells float up in medium are collected, enriched by centrifugation, stained with PI, and counted with flow cytometry. As irradiation time increases from 0, 1, 5, to 15 min, more cells are killed (Fig. 5D). Cells with negatively charged nanoparticles and X-ray are tested as comparison, where less cells are killed even when radiation condition is the same.

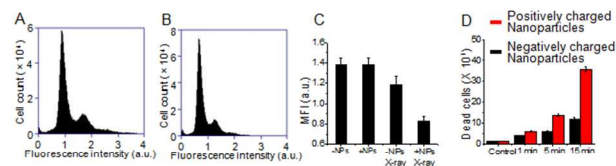


Figure 5. X-ray induced DNA damage of cells with negatively charged (A) and internalized (B) nanoparticles; MFI of cells after different treatment (C); Apoptosis cell counting (D).

DNA damage has been assessed at single cell level using HaloChip assay.<sup>26</sup> Briefly, cells with different treatments are attached on a solid substrate to form single cell array, and embedded in an agarose gel. After gel solidification, the sample is immersed in an aqueous solution of NaOH for lysis. Damaged DNA fragments will self-diffuse into gel matrix, forming a diffusive ring around nucleus. After staining cells with SYBR dye, DNA damage is quantified with relative nuclear diffusion factor (rNDF), which is derived from areas of halo and nucleus as follows:

$$\text{rNDF} = (R^2 - r^2)/r^2$$

where  $R$  and  $r$  are the radii of halo and nucleus, respectively. Fig. 6A-D show the fluorescence images of four samples, where each image (A-D) is from each sample (1-4). Fig. 6E shows rNDFs of cells after different treatment, where cells with internalized nanoparticles and X-ray irradiation have an rNDF of  $4.52 \pm 0.18$ , which is larger than those of cells with negatively charged nanoparticles ( $1.47 \pm 0.08$ ), cells with internalized nanoparticles ( $1.51 \pm 0.10$ ), and cells with negatively charged nanoparticles and with X-ray ( $2.41 \pm 0.07$ ). At last, DNA double strand break has been assessed with expression of a DNA repair protein,  $\gamma\text{-H2AX}$ . Primary and fluorescent labeled secondary antibodies are added



sequentially into culture media, and cells are imaged with fluorescence microscope. Fig. 6F-I show the fluorescence images of four samples, where each image (F-I) is from each sample (1-4). Cells with negatively charge nanoparticles (Fig. 6F), and internalized nanoparticles (Fig. 6G) show no fluorescence signal, indicating almost no  $\gamma$ -H2AX is expressed. Cells with negatively charged nanoparticles and X-ray show low level of fluorescence (Fig. 6H). Cells with X-ray and internalized nanoparticles show an increased fluorescence signal (Fig. 6I), indicating an increased expression of  $\gamma$ -H2AX. The expression of  $\gamma$ -H2AX protein is quantified with a 96 plate reader under an excitation light of 488 nm. Fig. 6J shows that cells with nanoparticles and X-ray show 170% higher intensity than those treated with X-ray alone, indicating enhanced DNA damage.

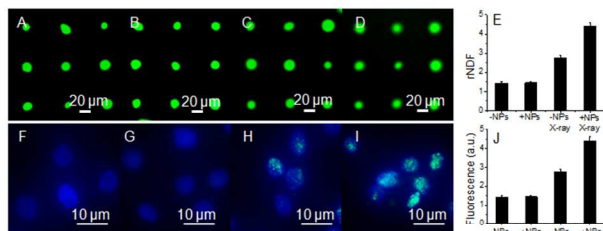


Figure 6. Fluorescence images of four samples after HaloChip assay (A-D), and their rNDFs (E); Immuno-staining of  $\gamma$ -H2AX protein in four samples (F-I), and according fluorescence intensity (J).

## Conclusions

A nanoparticle-based method is developed to enhance X-ray dose in radiation therapy by internalization of polyelectrolyte modified nanoparticles into cancer cells. Gold nanoparticles modified with positively charged polyelectrolyte have shown high cell membrane penetrating ability than those with negatively charged ones. The internalized nanoparticles do not change cell cycle, and can enhance X-ray radiation treatment of cancer, causing more DNA damage and cell death compared to those with negatively charged nanoparticles.

## Acknowledgements

This project is supported by a Director's New Innovator Award from National Institute of Health (1DP2EB016572).

## AUTHOR INFORMATION

### Corresponding Author

For nanoparticle enhanced radiation: [msu2@wpi.edu](mailto:msu2@wpi.edu)

For HaloChip assay: [lma2@wpi.edu](mailto:lma2@wpi.edu)

## Notes and references

- 1 F. Mark, U. Becker, J. N. Herak and D. Schultefrohlinde, *Radiat. Environ. Biophys.*, 1989, **28**, 81-99.
- 2 G. Pratviel, J. Bernadou and B. Meunier, *Angew. Chem. Int. Ed.*, 1995, **34**, 746-769.
- 3 W. K. Pogozelski and T. D. Tullius, *Chem. Rev.*, 1998, **98**, 1089-1107.

- 4 C. Chatgialiloglu and P. O'Neill, *Exp. Geront.*, 2001, **36**, 1459-1471.
- 5 M. Dizdaroglu, P. Jaruga, M. Birincioglu and H. Rodriguez, *Free Radic. Biol. Med.*, 2002, **32**, 1102-1115.
- 6 S. S. Wallace, *Free Radic. Biol. Med.*, 2002, **33**, 1-14.
- 7 C. Borek, *J. Nutr.*, 2004, **134**, 3207s-3209s.
- 8 B. F. Godley, F. A. Shamsi, F. Q. Liang, S. G. Jarrett, S. Davies and M. Boulton, *J. Biol. Chem.*, 2005, **280**, 21061-21066.
- 9 A. Akar, H. Gumus and N. T. Okumusoglu, *Appl. Radiat. Isot.*, 2006, **64**, 543-550.
- 10 Z. Goldberg and B. E. Lehnert, *Int. J. Oncol.*, 2002, **21**, 337-349.
- 11 J. F. Hainfeld, D. N. Slatkin, T. M. Focella and H. M. Smilowitz, *Br. J. Radiol.*, 2006, **79**, 248-253.
- 12 T. Kong, J. Zeng, X. P. Wang, X. Y. Yang, J. Yang, S. McQuarrie, A. McEwan, W. Roa, J. Chen and J. Z. Xing, *Small*, 2008, **4**, 1537-1543.
- 13 S. J. McMahon, W. B. Hyland, M. F. Muir, J. A. Coulter, S. Jain, K. T. Butterworth, G. Schettino, G. R. Dickson, A. R. Hounsell, J. M. O'Sullivan, K. M. Prise, D. G. Hirst and F. J. Currell, *Radiother. Oncol.*, 2011, **100**, 412-416.
- 14 E. Porcel, S. Liehn, H. Remita, N. Usami, K. Kobayashi, Y. Furusawa, C. Le Sech and S. Lacombe, *Nanotechnology*, 2010, **21**.
- 15 M. Alqathami, A. Blencowe, U. J. Yeo, R. Franich, S. Doran, G. Qiao and M. Geso, *J. Phys.: Conf. Ser.*, 2013, **444**.
- 16 Y. Luo, M. Hossain, C. M. Wang, Y. Qiao, J. C. An, L. Y. Ma and M. Su, *Nanoscale*, 2013, **5**, 687-694.
- 17 B. L. Jones, S. Krishnan and S. H. Cho, *Med. Phys.*, 2010, **37**, 3809-3816.
- 18 E. Lechtman, N. Chattopadhyay, Z. Cai, S. Mashouf, R. Reilly and J. P. Pignol, *Phys. Med. Biol.*, 2011, **56**, 4631-4647.
- 19 M. Hossain and M. Su, *J. Phys. Chem. C*, 2012, **116**, 23047-23052.
- 20 N. L. Rosi, D. A. Giljohann, C. S. Thaxton, A. K. R. Lytton-Jean, M. S. Han and C. A. Mirkin, *Science*, 2006, **312**, 1027-1030.
- 21 D. A. Giljohann, D. S. Seferos, P. C. Patel, J. E. Millstone, N. L. Rosi and C. A. Mirkin, *Nano Lett.*, 2007, **7**, 3818-3821.
- 22 C. B. He, Y. P. Hu, L. C. Yin, C. Tang and C. H. Yin, *Biomaterials*, 2010, **31**, 3657-3666.
- 23 M. D. Massich, D. A. Giljohann, A. L. Schmucker, P. C. Patel and C. A. Mirkin, *ACS Nano*, 2010, **4**, 5641-5646.
- 24 E. C. Cho, J. W. Xie, P. A. Wurm and Y. N. Xia, *Nano Lett.*, 2009, **9**, 1080-1084.
- 25 G. Decher, *Science*, 1997, **277**, 1232-1237.
- 26 Y. Qiao, C. M. Wang, M. Su and L. Y. Ma, *Anal. Chem.*, 2012, **84**, 1112-1116.

**The table of contents entry**

Polyelectrolyte modified nanoparticles are delivered into cancer cells to enhance X-ray radiation therapy.

